Optical spectroscopy of Cr^{4+}-doped Ca_2GeO_4 and Mg_2SiO_4

M. F. Hazenkamp and H. U. Güdel
Institut für Anorganische, Physikalische und Analytische Chemie, Universität Bern, Freiestrasse 3, CH-3000 Bern 9, Switzerland

M. Atanasov
Institute of General and Inorganic Chemistry, Bulgarian Academy of Sciences, B1.11, Sofia 1113, Bulgaria

U. Kesper and D. Reinen
Fachbereich Chemie und Zentrum für Materialwissenschaften, Philipps-Universität, Hans-Meerwein-Strasse, D-35032 Marburg, Germany
(Received 27 June 1995; revised manuscript received 27 September 1995)

Polarized single crystal absorption spectra and luminescence spectra of Cr^{4+}-doped Ca_2GeO_4 and Mg_2SiO_4 are presented and discussed. The absorption spectra are analyzed using the angular overlap model (AOM). The agreement between the experimental and the AOM-calculated energies of the ligand field states is satisfactory. The ligand field parameters $10Dq$ and B are 8950 cm^{-1} and 540 cm^{-1} for Ca_2GeO_4 and 10 100 cm^{-1} and 560 cm^{-1} for Mg_2SiO_4, respectively. The $^3A_2 \rightarrow {}^1A_1$ transition appears as a Fano antiresonance in the spectrum of Cr^{4+}-doped Mg_2SiO_4. The luminescence spectra are assigned to a transition from an excited triplet state, which is definitely not mixed with ^1E contributions in Ca_2GeO_4. The luminescence spectra are surprisingly sharp. Possible explanations are discussed. The luminescence of Cr^{4+}-doped Ca_2GeO_4 is much less quenched at room temperature than in the Mg_2SiO_4 host. Finally, the spectroscopic properties of Cr^{4+}-doped materials are compared with those of other $3d^2$ ions in tetroxo coordination.

I. INTRODUCTION

The discovery of the Mg_2SiO_4:Cr^{4+} near infrared laser[1,2] has stimulated a lot of spectroscopic research on $3d^2$ ions in tetroxo coordination.[3–11] Recently, we have reported the luminescence properties of Cr^{4+}-doped Ca_2GeO_4, which has the olivine structure, the same as Mg_2SiO_4.[12] In contrast to Mg_2SiO_4, Cr^{4+} ions are easily stabilized in Ca_2GeO_4 and no large concentrations of Cr^{3+} ions are found in addition to the Cr^{4+} ions.[9] Moreover, the luminescence is much less quenched at room temperature than the luminescence of Cr^{4+}-doped Mg_2SiO_4, suggesting that Cr^{4+}-doped Ca_2GeO_4 might be a very promising laser material.[12]

The assignment of the luminescence transition of Cr^{4+}-doped systems has been the subject of much debate over the past years. For several Cr^{4+}-doped systems the luminescence transition has been assigned to the $^3T_2 \rightarrow {}^3A_2$ as well as the $^1E \rightarrow {}^3A_2$ transition or to a transition from a strongly mixed $^3T_2/{}^1E$ excited state.[4,5,12–16] For Cr^{4+}-doped olivines the confusion has been caused by the sharp luminescence spectra at low temperatures which suggest an intraconfigurational $^1E \rightarrow {}^3A_2$ transition. These sharp luminescence spectra are especially puzzling since the low temperature luminescence of other Cr^{4+}-doped host lattices like Zn_2SiO_4,[17] $Ca_2Al_2SiO_7$,[18] or $LiNbGeO_5$ (Ref. 19) is very broad and structureless.

In this contribution, we present polarized single crystal absorption spectra and luminescence spectra of Cr^{4+}-doped Ca_2GeO_4 and Mg_2SiO_4. The absorption spectra are analyzed in terms of the angular overlap model (AOM).[20] The spectral data of the two host lattices are compared with each other and with spectral data of other tetrahedrally coordinated $3d^2$ ions. In this way we hope to clarify some ambiguities which may still exist concerning the energy levels of Cr^{4+}-doped systems.

II. EXPERIMENT

A Ca_2GeO_4 powder doped with 0.1% Cr^{4+} was synthesized according to procedures described in Ref. 9. Small single crystals (about $0.5\times0.5\times1.0$ mm) were grown using the flux method with $CaCl_2$ as a flux medium. Crystals were obtained by slowly cooling the melt in an argon atmosphere from 1250 °C with 5 °C per hour. The nominal Cr concentration is 0.5%. The real concentration in the crystal is probably smaller. The synthesis of the Cr-doped Mg_2SiO_4 crystal has been described in Ref. 21. A small piece ($3\times3\times4$ mm) was cut from the large Czochralski grown crystal. The Cr concentration was determined to be 0.035%.[21] Extinction coefficients and oscillator strengths were calculated assuming that all Cr ions (0.5% for Ca_2GeO_4 and 0.035% for Mg_2SiO_4) are in the tetravalent state.

Ca_2GeO_4 and Mg_2SiO_4 both have the olivine structure. The space group is *Pnmb* and hence the crystals are biaxial.[22,23] The optical axes were determined with a polarization microscope. They were assigned to crystallographic axes by comparing their polarized absorption spectra with those of Cr^{4+}-doped Mg_2SiO_4 crystals in the literature. The polarized absorption spectra of the two materials show a striking similarity.[4,12]

The spectroscopic equipment which was used is the same as described in Ref. 8. Luminescence spectra were recorded under excitation with a He-Ne laser operating at 633 nm or with a Xe lamp, using a water filter and a Schott KG3 filter to eliminate IR light from the Xe lamp. Decay curves were measured under excitation with a pulsed Nd:YAG (yttrium aluminum garnet) laser pumped dye laser operating at 700

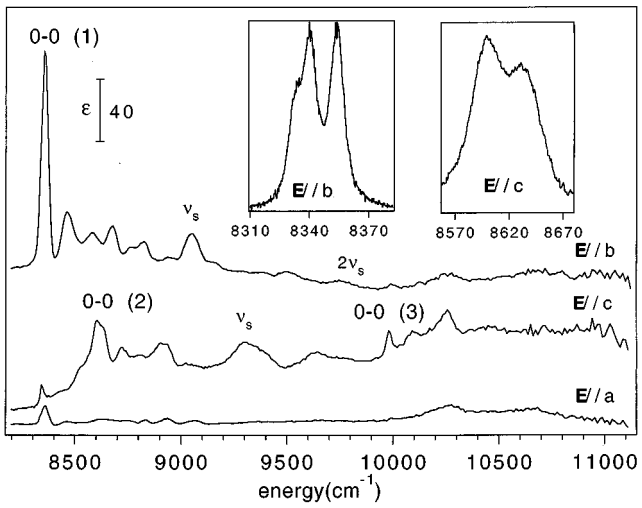

FIG. 1. Polarized absorption spectrum in the NIR of Cr^{4+}-doped Ca_2GeO_4 at 28 K with the electric vector parallel to the crystallographic a, b, and c axes. ε gives the molar extinction coefficient in 1 mole^{-1} cm^{-1}. The numbers of the three origins refer to Fig. 7. ν_s is the vibrational sideband due to coupling with the a_1 stretching vibration. The insets show the regions of the origins (1) and (2) under higher resolution.

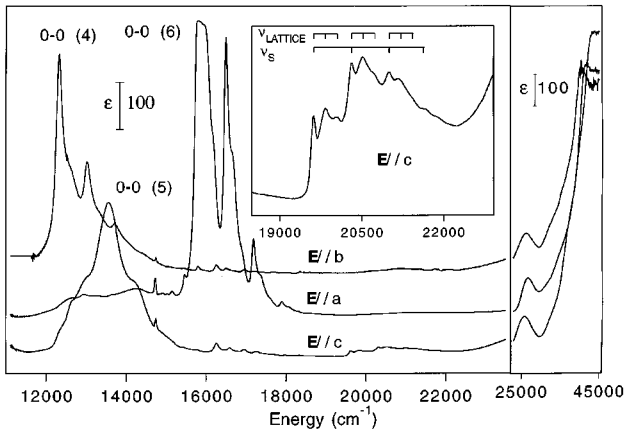

FIG. 2. Polarized absorption spectrum in the UV/VIS region of Cr^{4+}-doped Ca_2GeO_4 at 20 K. Note that the energy and intensity scales are different for the UV part of the spectrum. In the inset a part of the $\mathbf{E}\|c$ spectrum is magnified.

nm. The excitation spectrum in the visible region was measured using the light of a tungsten lamp which was dispersed through a Spex 1401 double monochromator. The luminescence was filtered through a near-infrared (NIR) cutoff filter (Germanium) before detection. The excitation spectrum in the ultraviolet region was measured on a Spex Fluorolog-2 spectrofluorometer, equipped with a Spex $N_{2(lq)}$-cooled Ge detector. In this case the sample was cooled using an Oxford flow cryostat.

AOM calculations were performed with the computer program AOMX developed by Adamsky[24] and with the program "Ligfield" developed by Bendix.[25]

III. RESULTS

A. The Ca_2GeO_4 host

Figure 1 shows the polarized absorption spectrum of Cr^{4+}-doped Ca_2GeO_4 in the near infrared at 28 K. It shows a pronounced polarization dependence. The lines at 8340 cm^{-1} for $\mathbf{E}\|b$, at 8610 and 9980 cm^{-1} for $\mathbf{E}\|c$ are assigned to the electronic origins of three separate transitions (1), (2), and (3), respectively. All other absorptions are vibrational sidebands of these origins. Coupling to a 700 cm^{-1} vibration can be observed for (1) and (2), indicated by ν_s in the figure [for (1) also by $2\nu_s$]. The Huang-Rhys factor $S(\nu_s)$ for coupling with ν_s is about 0.3 for transition (1). Under high spectral resolution the origins (1) and (2) show a triplet splitting of 22 cm^{-1} and a doublet splitting of 31 cm^{-1}, respectively. This is shown in the insets in Fig. 1.

In Fig. 2 the polarized absorption spectrum of Cr^{4+}-doped Ca_2GeO_4 in the UV/VIS (ultraviolet/visible) region at 20 K is presented. Three strong bands are observed with origins (4), (5), and (6) at 12320 cm^{-1} for $\mathbf{E}\|b$, at 13 550 cm^{-1} for $\mathbf{E}\|c$ and at 15 790 cm^{-1} for $\mathbf{E}\|a$, respectively. The transitions are almost completely polarized. In the absorption band (6) clear vibrational progressions are observed in a 700 cm^{-1} (ν_s) and a 200 cm^{-1} (ν_{lattice}) mode. Similar progressions are observed for the other two transitions (4) and (5), but less well resolved. $S(\nu_s)$ is about 0.4 for all three transitions. The zero-phonon transition of the absorption band (6) is cut off by stray light.

Weaker features appear at 14 730 cm^{-1} and around 20 000 cm^{-1}. The former transition is a sharp line occurring in all polarization directions. The latter, which is observed in the $\mathbf{E}\|c$ spectrum, is a structured band with the origin at 19630 cm^{-1} (see inset, Fig. 2). For this band two progressions can be distinguished in a 680 cm^{-1} (ν_s) and a 190 cm^{-1} (ν_{lattice}) mode. From the 680 cm^{-1} progression we derive a Huang-Rhys factor $S(\nu_s)$ of about 1.6.

The spectrum in the UV region (right part of Fig. 2) shows a broad structureless band at 26 000 cm^{-1}. At about 43 000 cm^{-1} a strong absorption band is observed in all polarization directions. The position and the intensity of this band cannot be accurately determined due to saturation effects. A series of weak lines appear between 16 000 cm^{-1} and 18 000 cm^{-1} for $\mathbf{E}\|b$ and $\mathbf{E}\|c$. It should be noted that several of these weak lines do not coincide with the strong sharp maxima of transition (6) in $\mathbf{E}\|a$ polarization. In Table I the energies of the zero-phonon transitions and the maxima of the observed bands in the absorption spectrum of Cr^{4+}-doped Ca_2GeO_4 are listed together with the oscillator strengths of the bands.

The unpolarized luminescence spectrum at 15 K of Cr^{4+}-doped Ca_2GeO_4 is shown in Fig. 3. The spectrum shows a sharp line at 8330 cm^{-1} and broader vibrational sidebands at lower energy. We also measured polarized luminescence spectra for $\mathbf{E}\|a$ and $\mathbf{E}\|b$. The luminescence transition appears to be predominantly $\mathbf{E}\|b$ polarized. High resolution luminescence spectra between 10 and 33 K reveal a triplet splitting of 22 cm^{-1} of the sharp luminescence origin. These three luminescence lines coincide with the three components of the lowest lying origin (1) in the near infrared absorption spectrum (see insets in Figs. 1 and 3). The high resolution luminescence spectra in the region of the origin were fitted to the sum of three Gaussians. Their relative integrated intensities were found to agree approximately to a Boltzmann distribution, assuming equal oscillator strengths

TABLE I. Experimental positions of electronic origins and band maxima, band intensities and band assignment of Cr^{4+}-doped Ca_2GeO_4.

0-0 transition (cm^{-1})	Band maximum (cm^{-1})	Symmetry label $C_s(T_d)$	Polarization	Oscillator strength
8 340	8 340	$^3A''(1)(^3T_2)$	$\mathbf{E}\|b$	6×10^{-5}
8 610	8 620	$^3A'(2)(^3T_2)$	$\mathbf{E}\|c$	5×10^{-5}
9 980	10 300	$^3A'(3)(^3T_2)$	$\mathbf{E}\|c$	4×10^{-5}
12 320	12 320	$^3A''(4)(^3T_1)(et_2)$	$\mathbf{E}\|b$	9×10^{-4}
13 550	13 550	$^3A'(5)(^3T_1)(et_2)$	$\mathbf{E}\|c$	8×10^{-4}
15 790	15 790	$^3A''(6)(^3T_1)(et_2)$	$\mathbf{E}\|a$	1×10^{-3}
14 730	14 730	$^1A'(^1A_1)$	$\mathbf{E}\|a,b,c$	9×10^{-6} ($\mathbf{E}\|a$)
19 630	20 500	$^3A'(^3T_1)(t_2{}^2)$	$\mathbf{E}\|c$	6×10^{-5}
	43 000	ligand to metal charge transfer	$\mathbf{E}\|a,b,c$	$10^{-1}-10^{-2}$
	26 000	$Cr(VI)O_4{}^{2-}$	$\mathbf{E}\|a,b,c$	

for the three transitions. When the temperature is increased to room temperature the luminescence spectrum broadens to a nearly structureless band.[12]

Luminescence decay times were measured of a polycrystalline Ca_2GeO_4 sample, nominally doped with 0.1% Cr^{4+} instead of the single crystal doped with 0.5% Cr^{4+} to avoid energy transfer among the Cr^{4+} ions. The luminescence spectra of the powder and the crystal are essentially the same.[13] The temperature dependence of the luminescence decay time and the integrated luminescence intensity are given in Fig. 4. Both quantities decrease by 30–40 % between 8 and 275 K.

Figure 5 shows the unpolarized excitation spectrum of the luminescence of Cr^{4+}-doped Ca_2GeO_4 at 15 K. Most of the bands which are observed in the absorption spectrum are also seen in the excitation spectrum. In particular, the weak sharp line at 14 730 cm^{-1} is clearly observed in the excitation spectrum and is shown on an expanded scale in the inset of Fig. 5. The broad structureless band at 26 000 cm^{-1} in the absorption spectrum (see Fig. 2) is not observed in the excitation spectrum of the Cr^{4+} luminescence.

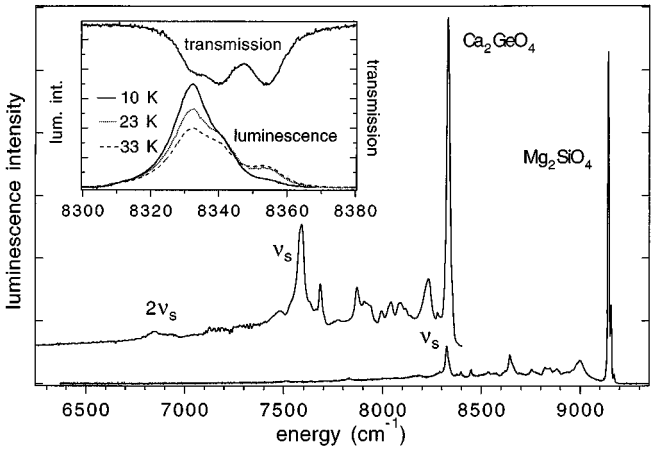

FIG. 3. Unpolarized luminescence spectra at 15 K of Cr^{4+}-doped Ca_2GeO_4 and Mg_2SiO_4. The two spectra are scaled to the same maximum intensity. The inset shows a high resolution transmission spectrum at 20 K of Cr^{4+}-doped Ca_2GeO_4 and high resolution luminescence spectra at several temperatures of the same compound in the origin region.

B. The Mg_2SiO_4 host

The polarized absorption and luminescence spectra of Cr^{4+}-doped Mg_2SiO_4 have been reported by several authors.[3,4,6,21] We reinvestigated this system and found essentially the same spectra as reported previously. As an illustration and for comparison with the Ca_2GeO_4 host spectra we present the polarized absorption spectrum of Cr^{4+}-doped Mg_2SiO_4 at 20 K in the visible region in Fig. 6. Three strongly polarized bands are observed in the visible region with very similar band shapes to the transitions (4), (5), and (6) for Cr^{4+}-doped Ca_2GeO_4. Accordingly, we also label them (4), (5), and (6), respectively, in Fig. 6. For Mg_2SiO_4, in contrast to Ca_2GeO_4, origin (6) is obviously not saturated with stray light due to the lower Cr^{4+} concentration. The main difference between the two host lattices is a shift of the absorption bands to higher energies for Mg_2SiO_4. In addition, the frequency of the vibration ν_s which couples to the transitions (4), (5), and (6) is larger for Mg_2SiO_4, viz. 750 cm^{-1} compared with 700 cm^{-1} for Ca_2GeO_4.

Two features in the absorption spectrum of Cr^{4+}-doped Mg_2SiO_4 have not been discussed before in the literature. First, a weak and slightly structured band with the origin at

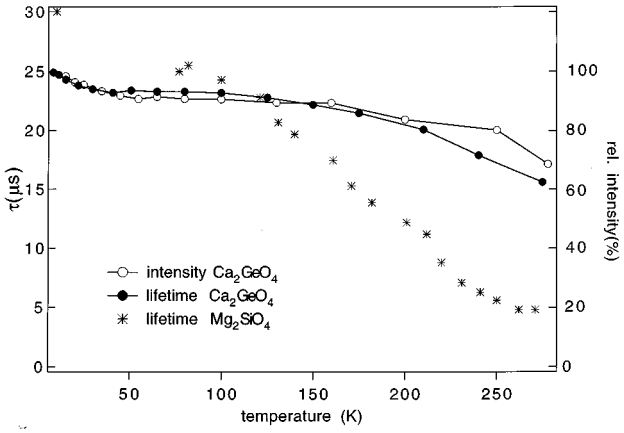

FIG. 4. Temperature dependence of the decay time and the integrated intensity of the luminescence of Cr^{4+}-doped Ca_2GeO_4 and of the luminescence decay time of Cr^{4+}-doped Mg_2SiO_4. The intensity is normalized at 10 K. The data of Mg_2SiO_4 were taken from Refs. 3 and 4.

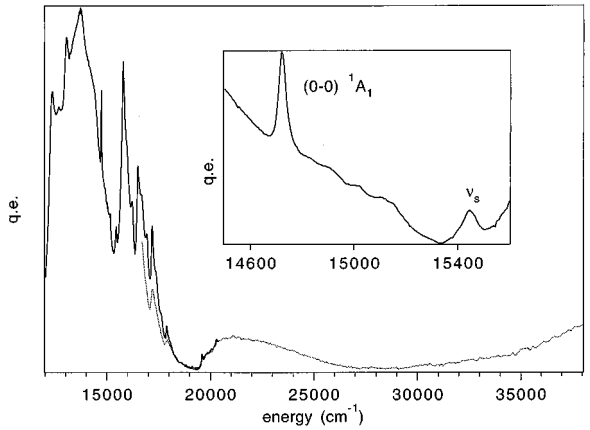

FIG. 5. Unpolarized excitation spectrum of the luminescence of Cr^{4+}-doped Ca_2GeO_4 at 15 K. The quantum efficiency (q.e.) is on an arbitrary scale. The spectra in the visible region (full line) and the UV region (dotted line) were measured on different setups. The inset shows the region of the $^3A_2 \rightarrow {}^1A_1$ transition on an expanded energy scale.

21 770 cm^{-1} is observed in the **E**$\|c$ spectrum (see inset Fig. 6). It is characterized by a much larger Huang-Rhys factor than the transitions (4)–(6), similar to the band with the origin at 19 630 cm^{-1} of Cr^{4+}-doped Ca_2GeO_4. Secondly, on the absorption band with origin (5) for **E**$\|c$ a structure is observed at about 15 240 cm^{-1}, which seems to be a ''dip'' in the broad absorption band.

The unpolarized luminescence spectrum of Cr^{4+}-doped Mg_2SiO_4 is compared with that of Cr^{4+}-doped Ca_2GeO_4 in Fig. 3. The band shape is very similar for the two systems. For the luminescence of Cr^{4+}-doped Mg_2SiO_4 the Huang-Rhys factor for coupling with the 815 cm^{-1} vibration $S(\nu_s)$ is about 0.2. Analogous to the case of Ca_2GeO_4, it is found that the origin of the luminescence band of Cr^{4+}-doped Mg_2SiO_4 coincides with that of the lowest absorption band (1).[4] In this system the origin shows a triplet splitting of 30 cm^{-1}. The higher two components of this triplet are occupied at higher temperatures according to a Boltzmann distribution.[4] The temperature dependence of the luminescence decay time of Cr^{4+}-doped Mg_2SiO_4 was taken from

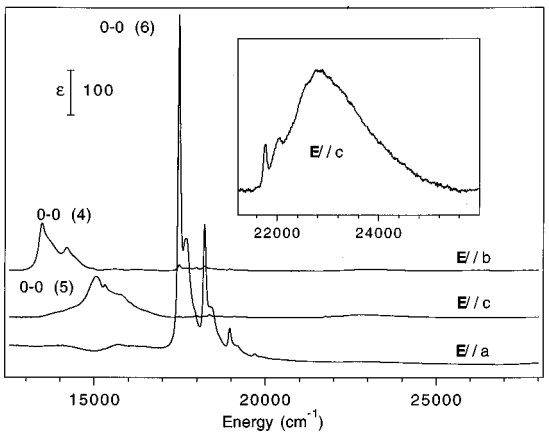

FIG. 6. Polarized absorption spectrum at 20 K in the visible region of Cr^{4+}-doped Mg_2SiO_4 for **E**$\|c$. In the inset a part of the spectrum is magnified.

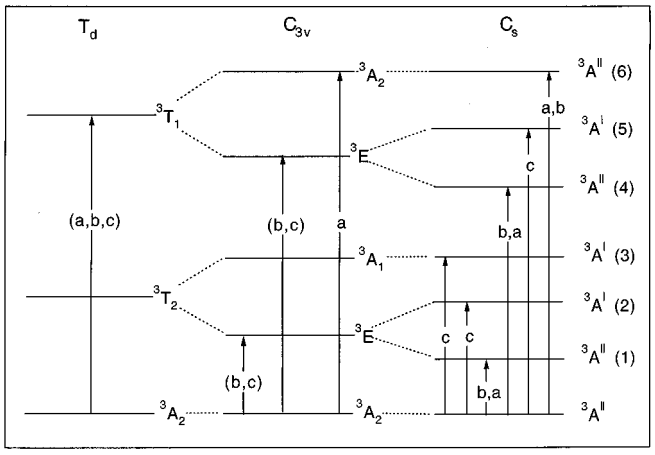

FIG. 7. Energy level diagram and selection rules for the electric dipole allowed transitions of Cr^{4+} when the site symmetry is lowered from T_d through C_{3v} to C_s. Absent arrows indicate forbidden transitions.

the literature and is included in Fig. 4.[3,4] The decay time decreases by about 90% between 10 and 275 K.

IV. ANALYSIS AND DISCUSSION

A. Spectroscopic assignments

It is assumed that the Cr^{4+} ion substitutes for the Ge(Si) ion in the olivine structure which is tetrahedrally coordinated. From the Tanabe-Sugano diagram we expect to observe absorption transitions from the $^3A_2$ ground state to the following excited states in our spectra (T_d labels): $^3T_2, {}^1E, {}^3T_1(et_2), {}^1A_1, {}^1T_2, {}^1T_1, {}^3T_1(t_2^2)$. We assume that the CrO_4 tetrahedron adopts the site symmetry of the Ge(Si)O_4 unit in the olivine structure. This tetrahedron shows a trigonal C_{3v} elongation along the crystallographic a axis with a smaller C_s component superimposed, leaving a mirror plane in the ab plane as the only symmetry element.[22,23] In Fig. 7 the energy levels, selection rules and the predicted polarization behavior of the $^3A_2 \rightarrow {}^3T_2$ and $^3A_2 \rightarrow {}^3T_1(et_2)$ transitions of Cr^{4+} are shown when the site symmetry is lowered from T_d through C_{3v} to C_s. For all the transitions only coupling with a_1 vibrational modes is expected, since there is no orbital degeneracy left.

We assign the origins (1), (2), and (3) in the absorption spectrum of Cr^{4+}-doped Ca_2GeO_4 (Fig. 1) to the transitions to the three orbital components $^3A''$, $^3A'$, and $^3A'$ of the $^3T_2$ state in C_s, respectively. The labels (1)–(3) are also used in Fig. 7 to identify the transitions. The polarization behavior of these three transitions roughly agrees with the approximate C_{3v} site symmetry. Details are understood considering the actual C_s site symmetry (see Fig. 7). In Ref. 12 the NIR absorption spectrum is discussed in more detail. The triplet splitting of 22 cm^{-1} of origin (1) and the doublet splitting of 31 cm^{-1} of origin (2) are due to a splitting of the $^3A''$ and $^3A'$ excited states, respectively. These splittings are caused by the combined action of spin-orbit coupling and the low symmetry ligand field. They can be well accounted for by the AOM calculations; see Sec. IV B. The zero field splitting of the $^3A_2$ ground state of Cr^{4+} in Ca_2GeO_4 has been reported to be much smaller, viz. 0.13 cm^{-1}.[9] Theoretically, three compo-

nents are expected for both origins. The third component is probably not resolved for origin (2) due to the broadening of the lines.

The three strong bands with origins (4), (5), and (6) in the visible absorption spectrum of Cr^{4+}-doped Ca_2GeO_4 are assigned to the transitions to the three orbital components of the ${}^3T_1(et_2)$ excited state. As expected these transitions are stronger than those of ${}^3A_2 \rightarrow {}^3T_2$, since the latter transition is forbidden in pure T_d symmetry. Their polarization behavior is in accordance with group theory (see Fig. 7). The total orbital splitting of the ${}^3T_1(et_2)$ state of about 3500 cm^{-1} is very large, but it can be well accounted for by the AOM calculations presented in Sec. IV B. The 700 and 200 cm^{-1} modes which couple to the three transitions (4), (5), and (6) are assigned to the a_1 stretching mode of the CrO_4^{4-} unit and a lattice mode, respectively.

The weak, structured band in the $\mathbf{E}\|c$ spectrum of Cr^{4+}-doped Ca_2GeO_4 with the origin at 19 630 cm^{-1} is assigned to the ${}^3A''({}^3A_2) \rightarrow {}^3A'({}^3T_1)(t_2{}^2)$ transition. Such an $e^2 \rightarrow t_2{}^2$ transition is weak since it involves a two electron excitation. $e^2 \rightarrow t_2{}^2$ transitions show a stronger dependence on the crystal field than $e^2 \rightarrow et_2$ transitions. Hence the Huang-Rhys factor $S(\nu_s)$ is larger compared with the $e^2 \rightarrow et_2$ transitions, viz. 1.6 vs 0.4, respectively. The weak sharp line which is observed in all polarization directions in the absorption spectrum and in the excitation spectrum at 14 730 cm^{-1} is ascribed to the spin forbidden, intraconfigurational ${}^3A_2 \rightarrow {}^1A_1$ transition. The strong absorption band at about 43 000 cm^{-1} is assigned to a ligand to metal charge transfer transition of Cr^{4+}.

The weak lines in $\mathbf{E}\|b$ and $\mathbf{E}\|c$ polarizations in the spectrum of Ca_2GeO_4 around 17 000 cm^{-1} might be due to some forbidden transition, e.g., the ${}^3A_2 \rightarrow {}^1T_2$ transition. However, we cannot exclude other explanations. They might, for example, be due to the ${}^3A''({}^3A_2) \rightarrow {}^3A''(6)({}^3T_1)(et_2)$ transition of Cr^{4+} ions in irregularly distorted tetrahedral sites. Note that a very similar pattern of weak lines is observed for the Mg_2SiO_4 host around 18 000 cm^{-1}. Because their assignment is ambiguous we shall not include these weak features in the ligand field analysis of Sec. IV B. The broad band around 26 000 cm^{-1} in the UV part of the absorption spectrum of Cr^{4+}-doped Ca_2GeO_4 is most probably not due to Cr^{4+} since it does not appear in the excitation spectrum of the Cr^{4+} luminescence. This band is ascribed to the ${}^1A_1 \rightarrow {}^1T_2$ charge transfer transition of $Cr(VI)O_4^{2-}$, which is present as a small impurity in the sample.[26] In Table I the assignment of the absorption bands of Cr^{4+}-doped Ca_2GeO_4 is summarized.

The absorption bands of Cr^{4+}-doped Mg_2SiO_4 due to the ${}^3A_2 \rightarrow {}^3T_2$ and ${}^3T_1(et_2)$ transitions have been identified by Jia *et al.*[4] The assignment runs parallel with that of Ca_2GeO_4. In addition, two more transitions occur in the absorption spectrum in the visible region for $\mathbf{E}\|c$ polarization at 20 K (see Fig. 6), from which the weak and slightly structured absorption band with origin at 21 770 cm^{-1} (see inset in Fig. 6) is ascribed to the ${}^3A_2 \rightarrow {}^3A'({}^3T_1)(t_2{}^2)$ transition.

We assign the dip at 15 240 cm^{-1} in the broad absorption band in the $\mathbf{E}\|c$ spectrum to Fano antiresonance of the sharp forbidden ${}^3A''({}^3A_2) \rightarrow {}^1A'({}^1A_1)$ transition with the broad transition due to the ${}^3A'' \rightarrow {}^3A'(5)({}^3T_1)(et_2)$ transition. Fano antiresonance is described as a destructive interference

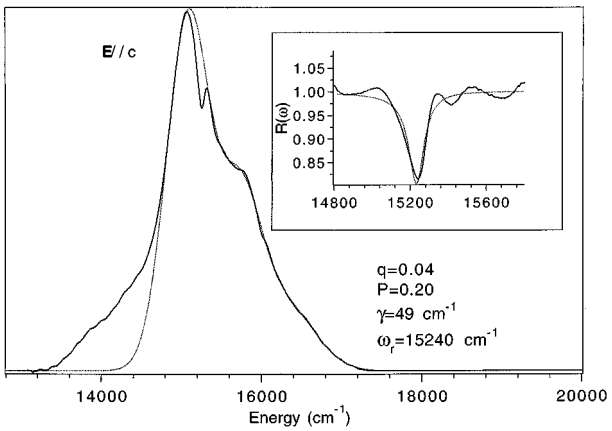

FIG. 8. Analysis of the Fano antiresonance profile in the absorption spectrum of Cr^{4+}-doped Mg_2SiO_4 (see Fig. 5). The dashed line is a triple-Gauss function which represents the background. The inset shows the ratio of the absorption band to the background, $R(\omega)$, with a fit to Eq. (1) (dashed line). The values of the fit parameters are given in the figure.

between a sharp forbidden transition to an excited state s and a broad allowed transition to an excited state b, resulting in a "dip" in the absorption spectrum.[27–30] We have analyzed the antiresonance profile applying the Fano theory adapted by Sturge *et al.*[27] The ratio of the observed absorption profile to the background, $R(\omega)$, is

$$R(\omega) = 1 + P\,\frac{(q^2 + 2\xi q - 1)}{1 + \xi^2}, \tag{1}$$

where

$$\xi = \frac{\omega - \omega_r}{\gamma}.$$

In the present case the s state (${}^1A_1$) and the b state [${}^3A'(5)({}^3T_1)(et_2)$] are interacting via spin orbit coupling. This interaction Hamiltonian connects the s state to a certain fraction P of the b state. γ gives the width of the sharp transition and is related to the strength of the spin orbit interaction between the s and the b state. q is a parameter which describes the shape of the resonance profile. ω_r is the resonance frequency, which is slightly different from ω_s, the energy of the transition to the unperturbed s state. The energy difference between ω_r and ω_s is usually denoted as the Lamb shift.[27–29]

The analysis of the antiresonance profile is illustrated in Fig. 8. The wings of the absorption band were fitted to the sum of three Gaussians, resulting in the background (dashed curve in Fig. 8). It should be noted that the choice of the background is critical for the calculation of $R(\omega)$. In the present case a strong dip appears on a steeply rising edge of the broad band, which makes the choice of the background rather ambiguous and introduces a relatively large error in $R(\omega)$. The inset shows the ratio $R(\omega)$ and the fit to Eq. (1). The values of the fit parameters ω_r, P, γ, and q are also given in the figure.

For Cr^{3+} and V^{2+} doped systems antiresonances occur due to the overlap of the transition to the ${}^2E$ and ${}^2T_1$ states with the transition to the ${}^4T_2$ state.[27–29] The situation of these

TABLE II. Comparison of absorption band maxima at 28 K and calculated AOM energies of the ligand field transitions of Cr^{4+}-doped Ca_2GeO_4 and Mg_2SiO_4. For Ca_2GeO_4 the energies, were calculated with e_σ=8629 cm^{-1}, e_π=1438 cm^{-1}, and B=540 cm^{-1}. For Mg_2SiO_4 with e_σ=9735 cm^{-1}, e_π=1623 cm^{-1}, and B=555 cm^{-1}. For both systems $C=4.2B$ (the free ion ratio).

Symmetry label of transition in C_s (T_d) $^3A''(^3A_2)\rightarrow$	Experimental band maximum Ca_2GeO_4:Cr^{4+} (cm^{-1})	Calculated AOM energy Ca_2GeO_4:Cr^{4+} (cm^{-1})	Experimental band maximum Mg_2SiO_4:Cr^{4+} (cm^{-1})	Calculated AOM energy Mg_2SiO_4:Cr^{4+} (cm^{-1})
$^1A''(^1E)$		8 545		8 810
$^1A'(^1E)$		8 546		8 812
$^3A''(1)(^3T_2)$	8 340	8 355	9 150	9 396
$^3A'(2)(^3T_2)$	8 620	8 360	9 820	9 530
$^3A'(3)(^3T_2)$	10 300	9 331	11 500	10 516
$^3A''(4)(^3T_1)(et_2)$	12 320	12 382	13 600	13 631
$^3A'(5)(^3T_1)(et_2)$	13 550	12 741	15 100	14 393
$^3A''(6)(^3T_1)(et_2)$	15 790	15 972	17 460	17 483
$^1A'(^1A_1)$	14 730	14 195	15 240	14 858
$^1A''(^1T_2)$		16 781		18 152
$^1A'(^1T_2)$		16 869		18 193
$^1A'(^1T_2)$		17 827		19 246
$^3A'(^3T_1)(t_2^2)$	20 500	21 669	22 700	23 786

$3d^3$ ions in octahedral coordination is rather similar to ours. Hence comparable values for P and for γ are found, viz. 10–20 % and 25–130 cm^{-1}, respectively.[27–29] The value of 0.04 for q may be compared with the one which can be calculated independently from the Hilbert transform of the background absorption spectrum. According to Ref. 27 $q=G_1(\omega_s)/G_2(\omega_s)$, where $G_2(\omega)$ gives the background absorption spectrum which is a triple Gauss function in our case. $G_1(\omega)$ is calculated from the Hilbert transform of $G_2(\omega)$ by numerical integration. Since we do not know the exact value of ω_s, we calculate q assuming $\omega_s \approx \omega_r$ and obtain $q=0.11$. However, q is strongly dependent on the exact value of ω_s. If a Lamb shift of only 40 cm^{-1} is assumed, q is calculated to be 0.04, in good agreement with the value obtained from the fit of $R(\omega)$. The reasonable values for the various parameters describing the antiresonance profile strongly indicate that the structure on the absorption band in Fig. 6 is indeed due to an antiresonance effect.

The coincidence of the absorption and luminescence origins (see Fig. 3) of Cr^{4+}-doped Ca_2GeO_4 prove the identity of chromophore and luminophore in this material. This is confirmed by the similar vibrational sidebands in absorption and luminescence (see Figs. 1 and 3) and their dominant $\mathbf{E}\|b$ polarization in both experiments. The Boltzmann equilibrium between the three components (see inset, Fig. 3) of the origin in the luminescence spectrum proves the spin-triplet character of the luminescent excited state. Hence the luminescence transition is ascribed to the $^3A''(1)(^3T_2)\rightarrow{}^3A''(^3A_2)$ transition. The luminescence decay time of Cr^{4+}-doped Ca_2GeO_4 of 25 μs at 10 K is essentially radiative.[12] This radiative lifetime τ_r is one to two orders of magnitude shorter than τ_r for Mn^{5+} and Fe^{6+} doped in oxidic lattices.[8,10] For these latter two ions it is well established that the luminescence is due to the spin-forbidden $^1E\rightarrow{}^3A_2$ transition. The short radiative lifetime for Cr^{4+} confirms the spin-allowed nature of the luminescence transition. For Cr^{4+}-doped Mg_2SiO_4 the assignment of the luminescence transition is similar and has been confirmed by piezospectroscopic experiments and optical Zeeman measurements.[5,31]

We have thus localized the split components of $^3T_2$, $^3T_1(et_2)$, $^1A_1$, and $^3T_1(t_2^2)$ excited states for both systems from absorption and luminescence measurements. Note that the $^3A_2\rightarrow{}^1E$ transition cannot be identified in the absorption spectrum. The spin forbidden $^3A_2\rightarrow{}^1A_1$ transition is about two orders of magnitude weaker than the $^3A_2\rightarrow{}^3T_1(et_2)$ transition from which it steals intensity by spin orbit coupling. Its half-width of about 30 cm^{-1} is relatively large. If it is assumed that the $^3A_2\rightarrow{}^1E$ transition steals its intensity from the $^3A_2\rightarrow{}^3T_2$ transition, we estimate that the oscillator strength of the $^3A_2\rightarrow{}^1E$ transition is very small, of the order of 10^{-6}–10^{-7}, and thus not observable on top of a broad and strong $^3T_2$ absorption.

B. Ligand field analysis

We performed a ligand field analysis of the absorption spectra of Cr^{4+}-doped Ca_2GeO_4 and Mg_2SiO_4 on the basis of the angular overlap model (AOM) (Ref. 20) to confirm our assignment. The angular geometry of the tetrahedra of the hosts were taken from the literature and used as input. One e_σ and one e_π parameter were used to describe the Cr-O bonding. The C/B ratio was fixed to 4.2, the same as in the free ion.[9,32] The ratio e_π/e_σ was fixed to 1/6, the same as in Ref. 9. Spin orbit coupling was neglected at this stage. In Table II the calculated AOM energies are given for Cr^{4+}-doped Ca_2GeO_4, calculated with e_σ=8629 cm^{-1}, e_π=1438 cm^{-1}, and B=540 cm^{-1} and for Cr^{4+}-doped Mg_2SiO_4 calculated with e_σ=9735 cm^{-1}, e_π=1623 cm^{-1}, and B=555 cm^{-1}. $10Dq$ equals $(4/9)(3e_\sigma-4e_\pi)$, corresponding to values of 8949 cm^{-1} and 10 095 cm^{-1}, respectively.

The agreement between the observed transition energies and the calculated AOM energies is satisfactory (see Table II) and confirms our assignment. As expected, the AOM parameters and $10Dq$ are smaller for Ca_2GeO_4 than for Mg_2SiO_4, since the Cr-O bonds are longer if the Cr^{4+} ion substitutes for a Ge ion compared to a Si ion. The B values are about the same for the two host lattices.

The very large trigonal splitting of the $^3T_1(et_2)$ state is reproduced very well by the AOM calculation for both systems. The trigonal splitting of the $^3T_2$ state is underestimated by a factor of two in both cases. On the other hand, the calculated rhombic splittings are much smaller than the experimental values. Possibly, there is an effect of the second coordination sphere of the Cr^{4+} ions in the crystals on these splittings. Alternatively, we may explain the discrepancy by assuming that the geometry of the CrO_4^{4-} complex is slightly different from that of the host $Ge(Si)O_4^{4-}$ complex.

The present AOM analysis is not accurate enough to determine a reliable energy of the $^3A_2 \rightarrow {}^1E$ transition which could not be localized by experiment. In our calculation for Cr^{4+}-doped Mg_2SiO_4 the ^1E state is found to be the lowest excited state (see Table II), which is not in agreement with the assignment of the luminescence to the $^3A''(1)(^3T_2) \rightarrow {}^3A''(^3A_2)$ transition. It has been argued before that a better ligand field description for Cr^{4+}-doped systems is obtained by using three different B parameters instead of only one,[9] because it is expected that the nephelauxetic effect is different for the three configurations e^2, et_2, and t_2^2 ("symmetry restricted covalency").[33] The nephelauxetic effect is expected to be larger for the t_2^2 configuration than for the e^2 configuration, because the t_2 orbitals are $\sigma+\pi$ antibonding whereas the e orbitals are only π antibonding.

Moreover, for the $3d^2$ ions Mn^{5+} and Fe^{6+} in tetroxo coordination it was found that the ratio of the experimental $^1A_1$ and ^1E energies is considerably smaller than the ratio calculated with ligand field methods where only one B parameter is employed.[10,34] Apparently, one even has to use two different B parameters for two excited states which arise from the same e^2 configuration. In Ref. 35 it is suggested that this is due to a different extent of mixing of the two excited singlet states with low lying charge transfer states.

There is no doubt that the fit of the calculated to the experimental band positions can be considerably improved by using different B values.[9] In particular, the energy of the $^3A_2(e^2) \rightarrow {}^1E(e^2)$ with respect to the $^3A_2(e^2) \rightarrow {}^3T_2(et_2)$ transition is expected to be raised if the concept of a parameter set with a single B value is left. However, we refrain here from introducing additional parameters (e.g., additional B parameters or distortion angles) to our simple model. We feel that we would strain the model and not gain any more physical insight. It is significant that the model in its present simplicity is able to reproduce some of the main features of the optical absorption spectrum of Cr^{4+} in both Ca_2GeO_4 and Mg_2SiO_4. We will nevertheless keep in mind as a qualitative argument in the following discussion that B is presumably of varying magnitude for the different electronic states.

We may examine the effect of the inclusion of a nonzero value for the effective spin-orbit (LS) coupling constant ζ_{crystal} in our model. The LS coupling constant of the free ion $\zeta_{\text{free ion}}$ [$=340$ cm^{-1} (Ref. 32)] is assumed to be reduced in the crystal by a factor β, the nephelauxetic ratio, which is defined as $B_{\text{crystal}}/B_{\text{free ion}}$ and is equal to about 0.54 for both hosts [$B_{\text{free ion}}=1015$ cm^{-1} (Ref. 36)]. This results in a ζ_{crystal} of about 180 cm^{-1}. A model calculation with the parameter set $\zeta_{\text{crystal}}=180$ cm^{-1}, $C=4.2B$, and $e_\pi=1623$ cm^{-1} was performed in the region where the $^3T_2$ and ^1E states cross, when the e_σ parameter (given in units of B) is varied (Fig. 9). The angular geometry of the Mg_2SiO_4 host is used as input, but the essential features in Fig. 9 also hold for Ca_2GeO_4.

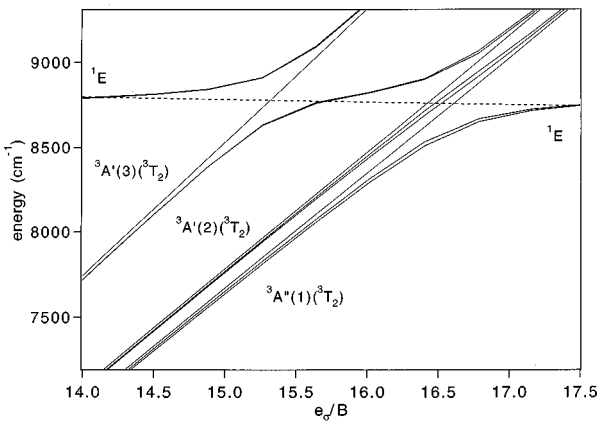

FIG. 9. Calculated energy level diagram for Cr^{4+}-doped Mg_2SiO_4 showing the influence of spin orbit coupling ($\zeta_{\text{crystal}}=180$ cm^{-1}) on the lower excited states when the AOM parameter e_σ is varied. The dashed curve shows the ^1E state for $\zeta_{\text{crystal}}=0$.

On the extreme left side in the diagram of Fig. 9 the ^1E state is well above all three orbital components of the $^3T_2$ state. Each of these components is split into three spinors due to the combined action of LS coupling and the crystal field. For $e_\sigma/B=14$ the splittings of the $^3A''(1)$, $^3A'(2)$, and $^3A'(3)$ states are calculated to be 27, 20, and 27 cm^{-1}, respectively. When e_σ/B increases, the ^1E state and the lower two spinors of the $^3A'(3)$ state mix. As a result, they repel each other and the lower two spinors of the $^3A'(3)$ state are lowered in energy. For $e_\sigma/B=15.6$ the $^3A'(3)$ state and the ^1E state are again a nearly pure triplet and singlet state, respectively, with the ^1E state lower in energy than the $^3A'(3)$ state. The calculated splittings of the $^3A''(1)$, $^3A'(2)$, and $^3A'(3)$ states are 48, 29, and 63 cm^{-1}, respectively. A similar mixing between the ^1E state and the $^3A'(2)$ and $^3A''(1)$ states takes place for $16<e_\sigma/B<17$. In this region the lower two spinors of the $^3A''(1)$ state are lowered in energy relative to the remaining third spinor of the $^3A''(1)$ state which is not perturbed by the interaction with the ^1E state. Hence the total LS splitting of the $^3A''(1)$ state increases for $e_\sigma/B>16$. For $e_\sigma/B>17$ a more or less pure ^1E state is the lowest excited state.

As was argued above, the e_σ/B ratio of 17.5 which results from the fit to the absorption band maxima of Cr^{4+}-doped Mg_2SiO_4 is not the correct value for this material since it is experimentally found that the ^1E is not the lowest excited state. We may compare the experimentally observed splittings of the orbital components of the $^3T_2$ state with the energy level diagram of Fig. 9, thereby trying to determine the appropriate e_σ/B ratios for our two systems. For the $^3A''(1)$ and $^3A'(2)$ states LS splittings of about 20–30 cm^{-1} are experimentally found for both Ca_2GeO_4 and Mg_2SiO_4. This appears to correspond with $e_\sigma/B \leqslant 15.6$ in Fig. 9, where the calculated total splittings of both orbital components are

smaller than 50 cm^{-1}. For $e_\sigma/B>15.6$ considerably larger splittings are predicted from Fig. 9. We conclude that the chosen B value used in the AOM calculation (555 cm^{-1} for Mg_2SiO_4) is too small to predict a reliable energy of the ^1E state. For this state we have to assume a larger B value. The increase can be estimated from the e_σ/B ratio of about 15.6 (see Fig. 9) in comparison to the experimental ratio of 17.5 to be about 11%, while from Table II one deduces an increase of only 3%—comparing the calculated and experimental energies for the $^3A_2(e^2)\rightarrow{}^1A_1(e^2)$ transition. Hence the $^3A_2\rightarrow{}^1E$ transition is expected to occur at about 9140 $\pm$340 cm^{-1} and 9430$\pm$350 cm^{-1} for Cr^{4+}-doped Ca_2GeO_4 and Mg_2SiO_4, respectively. It should thus appear well above the lowest $^3T_2$ split term in the case of Ca_2GeO_4. For Mg_2SiO_4 the estimated energy difference between ^1E state and the lowest $^3T_2$ split term is much smaller so that some $^1E-{}^3T_2$ interference cannot be definitely excluded in this case.

It should be noted that the $^3A_2\rightarrow{}^1E$ transition has never been unambiguously assigned in a spectrum of a Cr^{4+}-doped system. The sharp line luminescence of Cr-doped Ba_2TiO_4, which was claimed to be due to ^1E luminescence of Cr^{4+} centers,[37] was later shown to be due to a Mn^{5+} impurity.[38] Lines in the absorption spectra of Cr-doped YAG at about 8260 cm^{-1} (Ref. 7) and of Cr-doped MgCaBa aluminate glass at 8460 cm^{-1} (Ref. 16) have been tentatively assigned to the $^3A_2\rightarrow{}^1E$ transition of Cr^{4+} centers. However, these energies are similar to, or even lower than, the excitation energy of the ^1E state of Mn^{5+} in tetroxo coordination which ranges from 8300 to 9000 cm^{-1} for different host lattices.[8] The $^3A_2\rightarrow{}^1A_1$ transition, which is also a $e^2\rightarrow e^2$ transition, has a considerably higher energy for Cr^{4+} ($\approx$15 000 cm^{-1}) compared with Mn^{5+} [$\approx$13 500 cm^{-1} (Ref. 34)]. Therefore, it is expected that the $^3A_2\rightarrow{}^1E$ transition of Cr^{4+} also appears at a higher energy compared with Mn^{5+}. Luminescence experiments of several Cr^{4+}-doped materials at high hydrostatic pressure are in progress elsewhere,[39] in which it is tried to "push" the $^3A_2\rightarrow{}^3T_2$ transition to higher energies so that the ^1E state becomes the lowest (luminescent) excited state. This would thus allow a reliable determination of the energy of the ^1E state.

C. The luminescence transition

In Sec. IV A we have assigned the luminescence of both systems to the $^3A''(1)(^3T_2)\rightarrow{}^3A''(^3A_2)$ transition. Since this transition involves a change in the electronic configuration from et_2 to e^2, we expect broad band luminescence. At room temperature, broad luminescence bands are indeed observed for the two materials.[3,12] However, at 10 K the luminescence is very sharp; see Fig. 3. This is rather puzzling since the luminescence spectra of other Cr^{4+}-doped crystals like Zn_2SiO_4,[17] $Ca_2Al_2SiO_7$,[18] or $LiNbGeO_5$ (Ref. 19) consist of broad, structureless bands at all temperatures. It has repeatedly been suggested that the lowest excited state of Cr^{4+}-doped crystals is a strongly mixed $^3T_2/{}^1E$ state.[5,12–16] For the Cr^{4+}-doped olivines this might explain their sharp luminescence spectra.[12,13] In Sec. IV B we have provided evidence that the ^1E state lies at least several hundreds of cm^{-1} above the luminescent triplet state for Ca_2GeO_4, so that the luminescent state is a pure triplet state for this host. For Mg_2SiO_4 we cannot exclude that the lowest excited state is a mixed $^3T_2/{}^1E$ state (see Sec. IV B). However, similar narrow luminescence spectra are observed for both hosts so that singlet-triplet mixing cannot explain the narrow spectra of the two olivine hosts in comparison with the broad spectra of several other hosts.

We explain these very diverse luminescence band shapes by assuming that the main cause for the luminescence band broadening is coupling with bending vibrations. In Refs. 40 and 41 it is suggested that the coupling of totally symmetric as well as nontotally symmetric bending vibrations is a function of the static C_{3v} and C_s distortions of the CrO_4^{4-} tetrahedron. In Ca_2GeO_4 and Mg_2SiO_4 the trigonal and rhombic orbital splittings of the spin allowed transitions are very large, which suppresses the coupling of certain bending vibrations.[41] Hence the zero-phonon transition carries a great deal of intensity. It should be noted that weak coupling with bending vibrations is not only apparent for the luminescence transition, but also for several absorption transitions of these two materials. For example, the $^3A_2\rightarrow{}^3A''(6)(^3T_1)(et_2)$ transition is also very sharp. More experimental and theoretical[41] work is in progress to elucidate the mechanism of band broadening in these systems.

For both host lattices the decrease of the luminescence lifetime with increasing temperature is accompanied by a similar decrease in the integrated luminescence intensity (see Fig. 4 and Ref. 3). This is due to a nonradiative process. However, the temperature quenching is much stronger for Mg_2SiO_4 than for Ca_2GeO_4 (see Fig. 4). It is interesting to include in this discussion data of Cr^{4+}-doped $CaMgSiO_4$ and Mg_2GeO_4 which also have the olivine structure.[42,43] The temperature quenching is found to become stronger along the series Ca_2GeO_4, $CaMgSiO_4$, Mg_2GeO_4, Mg_2SiO_4. If we define the quenching temperature T_q by $\tau(T_q)=0.2*\tau(10\text{ K})$, where τ is the measured lifetime, then the quenching temperatures are 400, 320, 300, and 240 K, respectively. For Ca_2GeO_4 this value is a rather rough estimate, since we have no data for temperatures above 275 K. Due to the lack of data at 10 K for Mg_2GeO_4 we have defined T_q for this host by $\tau(T_q)=0.2*\tau(77\text{ K})$. We do probably not make a large error taking this definition for Mg_2GeO_4 since at 77 K the luminescence lifetime has apparently reached its low temperature plateau value.[43]

There is a clear relationship between the chemical composition of the host and the quenching temperature. The larger the cations in the olivine structure the higher the quenching temperature. The energy gap law, which is valid for weakly coupled systems,[44] predicts the quenching temperature to scale with $(1-\varepsilon^p)$.[45] ϵ is an empirical parameter with a value between 0 and 1, which is assumed to be the same for all host lattices and p is the number of phonons with energy $h\omega_{\text{acc}}$ that are needed to bridge the energy gap between the luminescence excited state and the ground state. Taking ν_s, as observed in the emission spectra of Cr^{4+}-doped Ca_2GeO_4 and Mg_2SiO_4 (see Fig. 3) as the accepting mode (740 and 820 cm^{-1}, respectively) and taking the 0-0 energy of the luminescence transition for the energy gap (8340 and 9150 cm^{-1}, respectively) we calculate for both hosts a value of p of about 11. We conclude that this primitive energy gap law cannot account for the significantly different quenching temperatures.

TABLE III. Comparison of experimental and structural data on several $3d^2$ ions in tetroxo coordination. The values for $B_{\text{free ion}}$ are taken from Ref. 36.

	V^{3+},[a]	Cr^{4+},[b]	Mn^{5+},[c]	Fe^{6+},[d]
$R_{\text{metal oxygen}}$ (Å)	1.84	1.76	1.70	1.65
$10Dq$ (cm^{-1})	≈8000	9000	11 000	13 000
B (cm^{-1})		540	500	375
$\beta=B_{\text{crystal}}/B_{\text{free ion}}$		0.54	0.42	0.27
E lowest LMCT (cm^{-1})		43 000	33 000	21 000
Oscill. strength $^3T_2$		5×10^{-5}	1×10^{-3}	8×10^{-3}
Oscill. strength $^3T_1(et_2)$		1×10^{-3}	9×10^{-3}	2×10^{-2}
Luminescence decay time at 10 K (μs)	11 (at 300 K)	25	400–1200	1600
First excited state	$^3T_2$	$^3T_2$	^1E	^1E

[a]Reference 11.
[b]This work, data on Ca_2GeO_4 and Ref. 9.
[c]References 8, 34, and 47.
[d]Reference 10.

More sophisticated models additionally introduce the Huang-Rhys parameter S to describe the temperature dependence of nonradiative rates.[45,46] From these models we expect a lower T_q for higher S. For the luminescence transition of Ca_2GeO_4 and Mg_2SiO_4 we have determined the Huang-Rhys parameter for coupling with ν_s. They are 0.3 and 0.2, respectively, i.e., the higher S, the higher the quenching temperature. This is opposite to what we would expect. It is obviously not straightforward to understand the different quenching temperatures for the four host lattices. The experimental trend along the chemical variable is very clear, however, and it can be used in the choice of host materials with high quenching temperatures.

D. Comparison with other d^2 ions

In Table III experimental spectroscopic data are compared for the series of $3d^2$ transition metal ions V^{3+}, Cr^{4+}, Mn^{5+}, and Fe^{6+}, all in tetroxo coordination. It should be noted that these data refer to ions doped into very diverse crystal structures, so that only the gross trends along the series may be discussed.

$10Dq$ increases along the series V^{3+}, Cr^{4+}, Mn^{5+}, Fe^{6+}. This trend is explained by the decreasing metal-oxygen distance R along the series (see Table III). Crystal field theory predicts $10Dq$ to scale with R^{-5}. However, the covalency is very pronounced and shows an increasing trend along the series of these tetroxo ions (see below), so that the application of crystal field theory is not really justified.

The Racah parameter B_{crystal} decreases along the series, which is remarkable since the values of $B_{\text{free ion}}$ follow an opposite trend.[36] This is illustrated in Fig. 10 where we have plotted for various $3d^2$ ions the experimental energy of the first excited singlet state (filled circles). In addition to data on the Cr^{4+}, Mn^{5+}, and Fe^{6+} ions in tetroxo coordination (first excited singlet state ^1E), also data on Ti^{2+} and V^{3+} in octahedral chloride coordination (first excited singlet state $^1T_{2g}$) are included in the figure. The open circles in Fig. 10 represent the steadily increasing ^1D energy of the free ions. Both the energies of the first excited singlet states and the energies of the free ion ^1D terms are in first approximation only dependent on B. The figure shows that for the ions Ti^{2+} and and V^{3+}, the increase of the ^1D energy cannot be offset by the nephelauxetic effect. The trend clearly turns around as we go to CrO_4^{4-}, MnO_4^{3-}, and FeO_4^{2-}. The reduction of the electron repulsion parameters due to increased covalency more than offsets the increase in the free ion values. The ^1E energy is reduced to less than 40% of its free ion value in FeO_4^{2-}. The result is a very pronounced decrease of the nephelauxetic ratio $\beta=B_{\text{crystal}}/B_{\text{free ion}}$ along the series in Table III. The increasing covalency along the series is also reflected by the decreasing energy of the first ligand to metal charge transfer transition (see Table III).

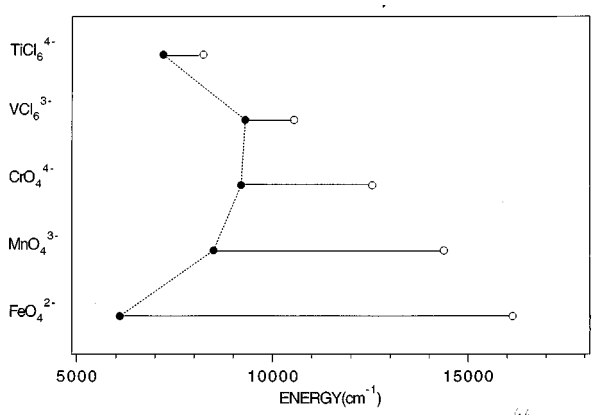

FIG. 10. $^1D-{}^3F$ energy differences (Ref. 36) of five free d^2 ions (empty circles) in comparison to the average $^3T_{1g}-{}^1T_{2g}(O_h$; Ti^{2+} and V^{3+}) or $^3A_2-{}^1E(T_d$; Cr^{4+}, Mn^{5+}, and Fe^{6+}) energy difference in crystals (filled circles). For Cr^{4+} the estimated $^3A_2-{}^1E$ energy is given; see Sec. IV B. References 48 and 49 were used for $MgCl_2$:Ti^{2+} and $Cs_2LiScCl_6$:V^{3+}, respectively.

The intensities of the spin allowed ligand field transitions increase along the above series. The $d-d$ transitions are Laporte forbidden, but can steal intensity from an allowed charge transfer transition by the crystal field. Hence the trend in the oscillator strengths of the ${}^3A_2 \rightarrow {}^3T_2, {}^3T_1(et_2)$ transitions is explained by the fact that the energy difference between the excited ligand field state and the lowest charge transfer state becomes smaller along the series.

Perhaps the most important change along the series occurs in the luminescence properties. For all the Fe^{6+} and Mn^{5+} systems studied so far the emitting state is ${}^1E$, while for all the Cr^{4+} and V^{3+} systems it is ${}^3T_2$. The different nature of the luminescence in Cr^{4+} and V^{3+} on the one hand and Mn^{5+} and Fe^{6+} on the other, is also reflected in the strongly increased lifetime of the excited state; see Table III. The crossing point in the Tanabe Sugano diagram of the ${}^1E$ and ${}^3T_2$ excited states occurs for $10Dq$ values which are slightly larger than typically found for Cr^{4+}.

V. SUMMARY AND CONCLUSIONS

We have presented and discussed the absorption and luminescence properties of Cr^{4+}-doped Ca_2GeO_4 and Mg_2SiO_4. The energies of the ligand field transitions of Cr^{4+}-doped Ca_2GeO_4 and Mg_2SiO_4 are reasonably well reproduced by a ligand field calculation on the basis of the AOM model. The values of the parameters B and $10Dq$ as well as the oscillator strengths of the spin allowed transitions fit nicely into trends observed for the series of other $3d^2$ ions in tetroxo coordination. Using ligand field considerations we have for both systems estimated the position of the ${}^1E$ excited state, which could not be identified by experiment. The NIR luminescence spectra of the two materials at 10 K are surprisingly sharp, but are nevertheless assigned to a spin allowed transition from the ${}^3A''({}^3T_2)$ excited state. Considering the estimated position of the ${}^1E$ excited state it follows that the narrow spectra are not likely caused by a strong mixing of the excited triplet state with the ${}^1E$ excited state. The luminescence of Cr^{4+}-doped Ca_2GeO_4 is much less quenched at room temperature than that of Cr^{4+}-doped Mg_2SiO_4 which suggests that Cr^{4+}-doped Ca_2GeO_4 might be a promising NIR laser material, on the conditions that crystals of high quality can be grown and that excited state absorption processes are not important.

ACKNOWLEDGMENTS

The authors would like to thank Dr. H. Rager of the Institut für Mineralogie, Petrologie und Kristallographie der Philipps Universität Marburg, Germany for providing the Cr^{4+}-doped Mg_2SiO_4 crystal, Dr. A. Meijerink of the Condensed Matter Department of the University Utrecht, the Netherlands for measuring the excitation spectrum in the UV region, and Dr. U. Oetliker for his help in the experimental work and for stimulating discussions. This work was financially supported by the Swiss National Science Foundation, the Human Capital and Mobility Program of the European Union, and the Deutsche Forschungsgemeinschaft.

[1] V. Petricevic, S. K. Gayen, and R. R. Alfano, Appl. Phys. Lett. **53**, 2590 (1988).
[2] H. R. Verdun, L. M. Thomas, D. M. Andrauskas, T. McCollum, and A. Pinto, Appl. Phys. Lett. **53**, 2593 (1988).
[3] V. Petricevic, S. K. Gayen, and R. R. Alfano, in *OSA Proceedings on Tunable Solid State Lasers*, edited by M. L. Shand and H. P. Jenssen (Optical Society of America, Woodbury, NY, 1989), Vol. 5, p. 77.
[4] W. Jia, H. Liu, S. Jaffe, W. M. Yen, and B. Denker, Phys. Rev. B **43**, 5234 (1990).
[5] W. Jia, H. Liu, Y. Wang, U. Hömmerich, H. Eilers, K. Hoffman, and W. M. Yen, J. Lumin. **59**, 279 (1994).
[6] R. Moncorge, G. Cormier, D. J. Simkin, and J. A. Capobianco, IEEE J. Quantum Electron. **27**, 114 (1991).
[7] H. Eilers, U. Hömmerich, S. M. Jacobsen, W. M. Yen, K. R. Hoffman, and W. Jia, Phys. Rev. B **49**, 15 505 (1994).
[8] U. Oetliker, M. Herren, H. U. Güdel, U. Kesper, C. Albrecht, and D. Reinen, J. Chem. Phys. **100**, 8656 (1994).
[9] D. Reinen, U. Kesper, M. Atanasov, and J. Roos, Inorg. Chem. **34**, 184 (1995).
[10] T. C. Brunold, A. Hauser, and H. U. Güdel, J. Lumin. **59**, 321 (1994).
[11] B. H. T. Chai and X. X. Zhang, *Advanced Solid State Lasers*, OSA Technical Digest (Optical Society of America, Washington, DC, 1995), p. 289.
[12] M. F. Hazenkamp, U. Oetliker, U. Kesper, D. Reinen, and H. U. Güdel, Chem. Phys. Lett. **233**, 466 (1995).
[13] T. Brunold, M. Herren, U. Oetliker, H. U. Güdel, U. Kesper, C. Albrecht, and D. Reinen, J. Lumin. **60&61**, 138 (1994).
[14] U. Hömmerich, H. Eilers, S. M. Jacobsen, W. M. Yen, and W. Jia, J. Lumin. **55**, 293 (1993).
[15] K. R. Hoffman, U. Hömmerich, S. M. Jacobsen, and W. M. Yen, J. Lumin. **52**, 277 (1992).
[16] X. Wu, S. Huang, U. Hömmerich, W. M. Yen, B. G. Aitken, and M. Newhous, Chem. Phys. Lett. **233**, 28 (1995).
[17] R. G. Pappalardo, W. J. Miniscalo, T. E. Peters, and K. Lee, J. Lumin. **55**, 87 (1993).
[18] L. D. Merkle, T. H. Allik, and B. H. T. Chai, Opt. Mater. **1**, 91 (1992).
[19] R. Moncorgé, H. Manaa, and A. A. Kaminskii, Chem. Phys. Lett. **200**, 635 (1992).
[20] C. E. Schäffer and C. K. Jørgensen, Mol. Phys. **9**, 401 (1965).
[21] H. Rager, M. Taran, and W. Khomenko, Phys. Chem. Minerals **18**, 37 (1991).
[22] U. Shigekazu, U. Kazuyori, and K. Keiichi, Semento Gijutsu Nenpo **29**, 32 (1975).
[23] J. D. Birle, G. V. Gibbs, P. B. Moore, and J. V. Smith, Am. Mineral. **53**, 807 (1968).
[24] H. Adamsky, AOMX: A Fortran computer package, Institut Theoretische Chemie, Heinrich-Heine-Universität, 40225 Düsseldorf, Germany, 1993.
[25] J. Bendix (unpublished).
[26] A. B. P. Lever, *Inorganic Electronic Spectroscopy*, 2nd ed. (Elsevier, Amsterdam, 1984), p. 325.
[27] M. D. Sturge, H. J. Guggenheim, and M. H. L. Pryce, Phys. Rev. B **2**, 2459 (1970).

[28] A. Lempicki, L. Andrews, S. J. Nettel, B. C. McCollum, and E. I. Solomon, Phys. Rev. Lett. **44**, 1234 (1980).
[29] M. Voda, J. Garcia Sole, F. Jaque, I. Vergara, A. Kaminskii, B. Mill, and A. Butashin, Phys. Rev. B **49**, 3755 (1994).
[30] A. Meijerink and G. Blasse, Phys. Rev. B **40**, 7288 (1989).
[31] T. S. Rose, R. A. Fields, M. H. Whitmore, and D. J. Singel, J. Opt. Soc. Am. B **11**, 428 (1994).
[32] S. Bashkin and J. O. Stoner, Jr., *Atomic Energy-Level and Grotian Diagrams* (North-Holland, Amsterdam, 1982), Vols. 3 and 4.
[33] C. K. Jørgensen, *Orbitals in Atoms and Molecules* (Academic, New York, 1962).
[34] D. Reinen, H. Lachwa, and R. Allmann, Z. Anorg. Allg. Chem. **542**, 71 (1986).
[35] M. Atanasov, Chem. Phys. **195**, 49 (1995).
[36] C. E. Moore, *Atomic Energy Levels*, NSRDS-NBS 35 (US Governmental Printing Office, Washington, DC, 1971).
[37] R. G. Pappalardo, T. E. Peters, W. J. Miniscalco, and E. J. Alexander, J. Lumin. **59**, 113 (1994).
[38] M. F. Hazenkamp, U. Kesper, D. Reinen, and H. U. Güdel, J. Lumin. **63**, 177 (1995).
[39] U. Hömmerich and K. L. Bray (unpublished).
[40] M. Atanasov, Chem. Phys. Lett. **234**, 313 (1995).
[41] M. Atanasov and J. Degen (unpublished).
[42] H. Eilers, U. Hömmerich, S. M. Jacobsen, and W. M. Yen, Chem. Phys. Lett. **212**, 109 (1993).
[43] V. Petricevic, A. Seas, R. R. Alfano, M. R. Kotka, and M. H. Randles, *Advanced Solid-State Lasers and Compact Blue-Green Lasers*, Technical Digest, Vol. 2 Abstract ATuE1-1 (Optical Society of America, Washington, DC, 1993).
[44] H. W. Moos, J. Lumin. **1&2**, 106 (1970).
[45] C. Reber and H. U. Güdel, J. Lumin. **47**, 7 (1990).
[46] Several contributions in *Advances in Nonradiative Processes in Solids*, Vol. 249 of *NATO Advanced Study Institute, Series B: Physics*, edited by B. Di Bartolo (Plenum, New York, 1991).
[47] J. B. Milstein, J. Ackerman, S. L. Holt, and B. R. McGarvey, Inorg. Chem. **11**, 1178 (1972).
[48] S. M. Jacobsen, H. U. Güdel, and C. A. Daul, J. Am. Chem. Soc. **110**, 7610 (1988).
[49] C. Reber, H. U. Güdel, G. Meyer, T. Schleid, and C. A. Daul, Inorg. Chem. **28**, 3249 (1989).